MRS Advances © 2019 Materials Research Society
DOI: 10.1557/adv.2019.253

Fabrication and performance test of biodegradable supercapacitor

Hu Li,[1,2] Yubo Fan[1*] and Zhou Li[2,3*]

[1]*Beijing Advanced Innovation Centre for Biomedical Engineering, Key Laboratory for Biomechanics and Mechanobiology of Chinese Education Ministry, School of Biological Science and Medical Engineering, Beihang University, Beijing 100083, China. E-mail: yubofan@buaa.edu.cn*

[2]*CAS Center for Excellence in Nanoscience Beijing Key Laboratory of Micro-Nano Energy and Sensor, Beijing Institute of Nanoenergy and Nanosystems, Chinese Academy of Sciences, Beijing 100083, China.*

[3]*School of Nanoscience and Technology, University of Chinese Academy of Sciences, Beijing 100049, China. E-mail: zli@binn.cas.cn*

ABSTRACT

Power source plays an important role in keeping normal functions of biodegradable electronic devices. In this paper, we proposed a fabrication method of biodegradable supercapacitor (BSC), which can provide energy for portable and implantable medical electronics. The BSC has a sandwich-like symmetric structure, which was assembled layer by layer. The electrochemical performances of BSC were measured, including the cyclic voltammetry test, galvanostatic charge-discharge and electrochemical impedance spectroscopy. Titanium foil was used as a template to generate microstructure for polylactic acid (PLA) supporting substrate. The microstructure provided strong adhesion force for iron film in sputtering process. The nanoporous zinc oxide layer was prepared by evaporation-driven self-assembly technology on iron film. The nanoporous structure was in favour of ionic storage in charging-discharging process. About 60% of capacitance retention was achieved after 3000 times of cycling test. After connecting three BSC in series, a green LED pattern was lighted up immediately, indicating that the energy was stored in BSC device successfully. After immersing the BSC in DMEM, the BSC can be totally degraded gradually. This work provided a feasible scheme for developing biodegradable energy storage device, it also gave a possible avenue for powering biodegradable electronic devices.

INTRODUCTION

With the fast development of electronic products, various innovative energy harvesting and storage technologies emerged to meet their power requirements.[1-3] As new electronic devices, biodegradable electronic devices (BEDs) can be partly or fully degraded in biofluid and environmental water, which is totally different from the durable operation of traditional electronic devices.[4-8] The BEDs can be used in implantable medical diagnose and therapy, avoiding the second operation and side-reaction of long-term implantation.[6-8] For military sensor application, the BEDs achieved instant degradation after being discarded, which contributed to enhancing information privacy.[9] They can also serve portable consumer electronics, which achieved self-degradation after being discarded and avoided the accompanying high collection cost.[10] For biodegradable electronic device, the biodegradable power source is an indispensable part for realizing normal operation of biodegradable electronic devices. Compared with wireless power supply, biodegradable implantable energy device should simultaneously meet strict requirements of miniaturization, good biocompatibility and bioabsorbability to realize the long-term implantation by minimally invasive surgery without removing in future.[11-13] However, researches about energy supply for biodegradable implantable electronics are very limited.

The commonly used energy storage device consisted of supercapacitor and battery. The supercapacitor has attracted much research interests for its fast charging-discharging rate.[14-15] Carbonized materials (carbon nanotube, active carbon, graphene and porous carbon) are usually used for supercapacitor as active material due to their excellent conductive property, large specific area and strong resistance to acidic/alkaline environment.[16-17] These features endow them with high specific capacitance and stable cycling performance. Acidic electrolytes (H_2SO_4 and H_3PO_4) and alkaline electrolytes (KOH) are preferred for their outstanding ionic mobility and low resistance. Whereas these components are unsuitable for implantation operation due to their nonbiodegradable and poor biocompatible properties.[18-19] Therefore, it is necessary to develop new type of supercapacitor for energy storage to meet the strict requirements of implantable and biodegradable electronics. In our previous work, a hydrothermal method was used to prepare nanopillar structure on supporting substrate to anchor electrode film, and phosphate buffered solution was used as mixed electrolyte.[6] Compared with the previous work, a template method by titanium foil in this work was used to directly fabricate microstructure on supporting substrate to anchor electrode film. Sodium chloride (NaCl) was used as pure electrolyte for its simple constituent. Additionally, the edges of supercapacitor were not packaged, and the device has a simpler structure to be assembled.

Specifically, the developed biodegradable supercapacitor (BSC) employed neutral electrolyte as positive and negative charge source. Polylactic acid (PLA) was selected as supporting material and protected the overall structural integrity of BSC in practical usage. Iron films served as positive and negative electrodes, respectively. Evaporation-driven technology was used to prepare nanoporous zinc oxide layer.[15] Polyvinyl Alcohol (PVA) hydrogel with sodium chloride was used as solid-state separator film and neutral electrolyte. A symmetric sandwich-like structure was built by assembling two same as-prepared samples layer by layer. Various characterizations proved the good electrochemical performance of the as-fabricated BSC. This BSC can store energy successfully in air and power green light-emitting diode (LED). After immersing the BSC in dulbecco's modified eagle medium (DMEM) solution, the device can be degraded under hydrolytic decomposition.

EXPERIMENTAL DETAILS

PLA granules were put on a heating titanium foil at 250 ℃ until they melt into transparent liquid. Then another titanium foil was pressed on the liquid to a proper thickness. The sample was put into deionized (DI) water to make it cooling. Peeling off the PLA film from titanium foil and used it as supporting substrate for iron sputtering. Supersaturated zinc oxide dispersion (10 mg/ml) in ethyl alcohol was dropwise added onto the iron film until a self-assembled zinc oxide layer formed. 20 mg of zinc oxide was added on each iron film. Some sodium chloride (NaCl) was added in polyvinyl acetate (PVA) hydrogel in DI water (mass fraction, 10 %) to prepare solid-state electrolyte (1 mol/L). The PVA was dissolved in DI water at 80 ℃ with intensely stirring.

The biodegradation of BSC was demonstrated in dulbecco's modified eagle medium (DMEM) at 80℃. The electrochemical performances of the as-fabricated supercapacitor were measured using electrochemical station (CHI660E) and impedance/gain-phase analyzer (solartron, SI1260) at room temperature. The surface morphologies of PLA film, iron film and self-assembled zinc oxide layer were characterized by scanning electron microscopy (SEM, HITACHI, SU8020).

RESULTS AND DISCUSSION

Assembly of BSC device

Figure 1 (a-b) shows the picture of as-fabricated biodegradable supercapacitor in air. Figure 1a shows two pieces of freshly-prepared half supercapacitor. The white component is self-assembled zinc oxide layer on iron film surface. Aluminum belt is attached on one side of the supercapacitor as leading wire. After adding polyvinyl acetate (PVA) hydrogel on the zinc oxide layer, two pieces of samples are pressed together into one integrated supercapacitor device (Figure 1b). The size of the BSC is 1.5 cm × 1.5 cm. This integrated supercapacitor is used for electrochemical performance test in the following parts. Figure 3c shows the degradation environment of BSC in DMEM in a six-well plate. The biodegradability demonstration of BSC was carried out in DMEM at 80 ℃ in a drying oven.

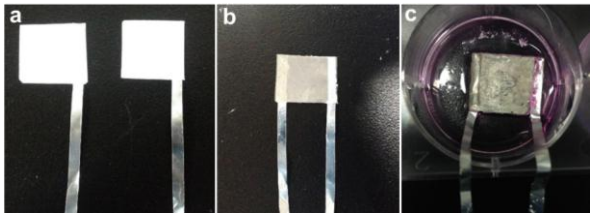

Figure 1. Schematic diagram of BSC assembly. (a) Picture of BSC with zinc oxide on iron film before assembly. b) Picture of integrated BC after assembly. (c) Picture of BC for degradation demonstration in DMEM.

Morphology characterization of BSC components

The components of BSC are characterized from bottom to up. The microstructure of active material played a key role in determining the specific

capacitance of BSC, which provides a relatively large area for charge storage. As shown in Figure 2 (a-c), SEM images with different magnification times present the self-assembled microstructure of zinc oxide layer on iron film. The edge of zinc oxide layer is a brushy fracture surface (Figure 2a). A magnified view shows micro pores inside the layer (Figure 2b). The cross section has a fluctuated and soft porous structure, indicating the large specific area in this self-assembled layer. A further magnified view (Figure 2c) contains various-sized zinc oxide particles. The small-sized particle can separate large pores into small pores, which in turn increase the specific area of self-assembled layer. In the charging-discharging process, the positive and negative charges constantly accumulated on the zinc oxide surface and migrated into PVA hydrogel. Meanwhile, the loose stack structure can also increase the specific area of self-assembled zinc oxide layer.

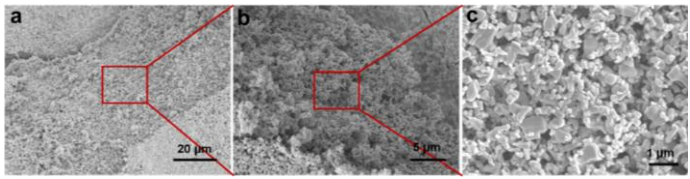

Figure 2. SEM images with different magnification of self-assembled zinc oxide layer. (a) Overall appearance of self-assembled zinc oxide layer. (b) A magnified view of the cross section. (c) Particle distribution in the inner space of self-assembled zinc oxide layer.

As shown in Figure 3, PLA film was prepared by pressing its melt granule on healing titanium film. The titanium acted as a template to generate micro-structure and anchor the iron film. Figure 3a shows the oriented strips along the left bottom to top right corner on PLA surface. The partial enlargement (Figure 3b) shows a fluctuated surface of PLA film. The further enlarged view (Figure 3c) indicates many concave-convex positions existed on PLA surface, which can provide strong adhesion force for iron film during magnetron sputtering process. As shown in Figure 3d, the oriented strips are partially covered after sputtering iron film on PLA supporting substrate. The surface of PLA-iron becomes more smooth. The roughness is lower than the primary PLA film (Figure 3e). The iron electrode is anchored on the PLA surface and shows a continuous structure (Figure 3f), which ensure good conductivity of BSC in charging-discharging process. The microstructure of PLA supporting substrate provides strong adhesion force to protect the iron film from falling off in practical usage.

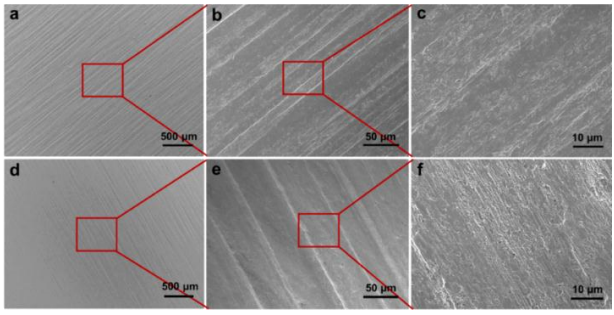

Figure 3. (a-c) Surface morphologies of PLA film with different magnification. (d-f) Surface morphologies of iron film on PLA supporting substrate with different magnification.

Electrochemical performance measurement

As shown in Figure 4, the electrochemical performances of the as-fabricated supercapacitor are measured by electrochemical station. The cyclic voltammetry (CV) curves (Figure 4a) at different scan rates from 10 mVs^{-1} to 300 mVs^{-1} show rectangle-shaped circles, indicating good electrochemical performance of the BSC in charging-discharging process. Galvanostatic charge/discharge (GCD) test (Figure 4b) shows triangle-like shape, indicating good ionic immigration in charging-discharging process. The specific capacitance based on GCD curves can be calculated according to the following formula:

$$C_m = \frac{I \cdot t}{m \cdot \Delta V}$$

where C_m is the specific capacitance, I is the applied current, t is the discharging time, m is effective mass of zinc oxide on each electrode, ΔV is the potential window. The specific capacitance value varied from 6.5 mF g^{-1} to 5 mF g^{-1} at the current density range from 0.5 mA g^{-1} to 5 mA g^{-1}, and a capacitance retention of 76.9% was obtained, indicating a good rate capacity.

The specific capacitance (Figure 4c) of BSC is calculated according to the following formula:

$$C_m = \frac{\int I \, dV}{v \cdot \Delta V \cdot m}$$

where C_m is the specific capacitance, I is the response current of ordinate, v is the scan rate, ΔV is the potential window, m is effective mass of zinc oxide on each electrode. Figure 4c shows that the specific capacitance of BSC gradually decreases with the increasing scan rates. A maximum capacitance value of 18 mF g^{-1} is obtained at 10 mV s^{-1}. When the scan rate is faster than 100 mV s^{-1}, the specific capacitance reaches to the stable value of about 9.8 mF g^{-1}, a capacitance retention of about 87.4% was obtained from 50 mV s^{-1} to 300 mV s^{-1}, indicating a good rate capacity. At the same time, we test its cycling performance in air for 3000 times (Figure 4d). The capacitance first decrease before 500 cycles due to incomplete activation of active material, then keep stable up to 3000 times. A capacitance retention of about 60% is achieved, which indicates a good cycling performance of the as-fabricated supercapacitor.

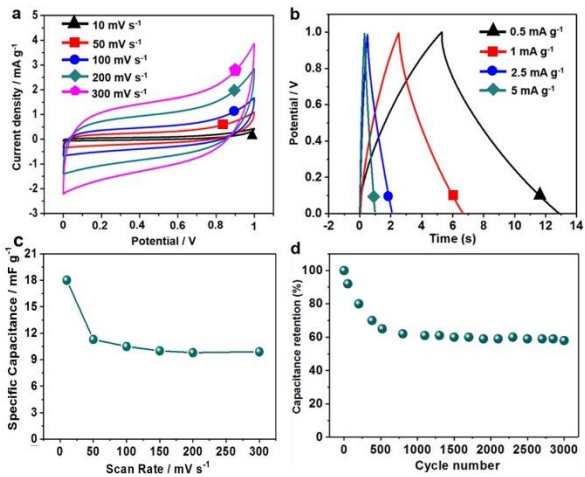

Figure 4. Electrochemical performance measurement of the as-fabricated supercapacitor. (a) CV curves of BSC at different scan rates from 10 to 300 mV s^{-1}. (b) GCD curves of BSC at different current densities from 0.5 to 5 mA g^{-1}. (c) Specific capacitance variation with scan rates. (d) Cycling performance test of BSC for 3000 times.

Electrochemical impedance spectroscopy measurement

Electrochemical impedance spectroscopy (EIS) measurement is carried out in the frequency range between 10 mHz and 100 kHz. The Z (Re) represents the real component in the complex plane, it shows the Ohmic property. −Z (Im) represents the imaginary component, it shows the capacitive property. The Nyquist plot of supercapacitor includes three parts, which are in connection with the frequencies. In the very high frequency area, the features of supercapacitor like a pure resistor. In the low frequency region, the imaginary part rapidly increases to a vertical line, it reflects the capacitive property. In the medium frequency region, it can reflect the influence of material porosity on capacitive property. When the frequency decreases from high to low, the signals penetrate into the self-assembled porous layer deeper and deeper. Then more and more zinc oxide surfaces become available for charge storage. The medium frequency region is in connection with the electrolyte penetration in porous structure. This region is commonly referred to as Warburg curve.[20] The EIS spectrum of BSC (Figure 5) shows a linear trend in the low frequency region, an arc-shaped curve or a similar arc-shaped curve in the high frequency region. In the low region, it is close to 90°, indicating good ionic propagation and immigration. The equivalent series resistance of BSC is about 180 Ω.

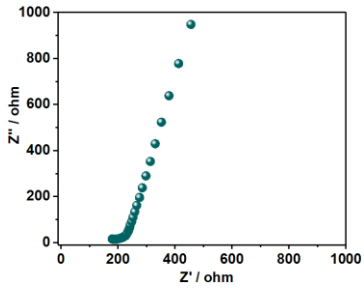

Figure 5. EIS curve of BSC in the frequency range between 10 mHz and 100 kHz.

Biodegradability demonstration of BSC in DMEM

To demonstrate the biodegradability of the as-fabricated BSC, the device is immersed in DMEM solution at 80 ℃. The DMEM is replaced with new solution every 24 hours. Figure 6a shows the primary structure of BSC before immersion in DMEM. After immersion for 1 day, the integrity of BSC is destroyed. PVA hydrogel dissolved into DMEM. The zinc oxide layer spread to surrounding solution. Parts of iron film fell off from PLA supporting substrate (Figure 6b). After 4 days, the PLA film changed from transparent to opaque. Some parts of PLA are broken (Figure 6c). After 6 days, the device broke into pieces. Iron film and zinc oxide layer disappeared due to the DMEM exchange (Figure 6d). After 8 and 10 days, the whole device broke into PLA powder and gradually disappeared in the following time. These results indicate that the as-fabricated BSC has a good biodegradability after usage.

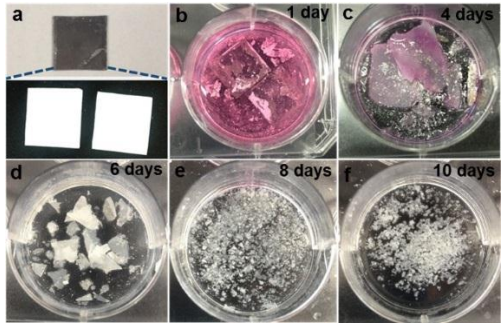

Figure 6. Degradability demonstration of the as-fabricated BSC in DMEM at 80℃. (a) Primary structure of the as-fabricated BSC. (b-f) Degradation images of BSC in DMEM for different days.

Application presentation of BSC

To prove the feasibility of using BSC to power portable electronics, three BSC devices are connected in series and then charged to 3 V in 40 s (Figure 7a). Then the tandem BSC is used to power a green light-emitting diode (LED) pattern. The pattern is immediately lighted up when turn on the tandem BSC. It indicates that energy is successfully stored in BSC and the supercapacitor can act as a power source for biodegradable electronics.

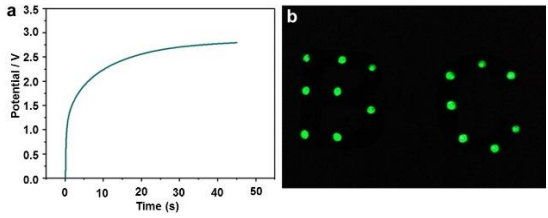

Figure 7. Application presentation of the as-fabricated BSC for powering green LED. (a) Charging curve of three BSCs in series. (b) Lighting up a green LED pattern using BSC.

CONCLUSIONS

In summary, a biodegradable supercapacitor was successfully developed for powering portable electronics. The BCS has a sandwich-like structure from top to bottom, including PLA supporting substrate, self-assembled zinc oxide layer, PVA hydrogel electrolyte. Various characterizations proved that the as-fabricated BCS has good electrochemical performance. The BSC has a maximum capacitance value of about 18 mF g^{-1} at 10 mV s^{-1}. It achieved good capacitance retention of about 60 % after 3000 cycles. After immersing BSC in DMEM at 80 ℃, it achieved a fast degradation in 10 days. After connecting BSC in series, it can light up a green LED pattern, which proved its feasibility as a power source for biodegradable electronic devices in future.

ACKNOWLEDGMENTS

The authors thank the support of National Key R&D Project from Minister of Science and Technology, China (2016YFA0202703), National Natural Science Foundation of China (Nos. 61875015, 31571006, 81601629, 21801019, 61501039, 11421202 and 11827803), the Beijing Natural Science Foundation (2182091), China Postdoctoral Science Foundation (2018M641148), Beijing Council of Science and Technology (Z181100004418004) and the National Youth Talent Support Program.

REFERENCES

1. F. Huang, M. J. Li, P. Siffalovic, G. Z. Cao, and J. J. Tian. Energy Environ. Sci. **12**, 518 (2019).
2. J. H. Wang, H. Wang, N. V. Thakor, and C. Lee. ACS Nano **13**, 3589 (2019).
3. J. P. Xie, Y. Q. Zhu, N. Zhuang, H. Lei, W. L. Zhu, Y. Fu, M. S. Javed, J. L. Li, and W. J. Mai. Nanoscale **10**, 17092 (2018).
4. M. Irimia-Vladu, E. D. Głowacki, G. Voss, S. Bauer, and N. S. Sariciftci, Mater. Today **15**. 340 (2012).
5. S. -W. Hwang, H. Tao, D. -H. Kim, H. Cheng, J. -K. Song, E. Rill, M. A. Brenckle, B. Panilaitis, S. M. Won, Y. -S. Kim, Y. M. Song, K. J. Yu, A. Ameen, R. Li, Y. Su, M. Yang, D. L. Kaplan, M. R. Zakin, M. J. Slepian, Y. Huang, F. G. Omenetto, and J. A. Rogers. Science **337**, 1640 (2012).
6. H. Li, C. C. Zhao, J. P. Meng, X. X. Wang, Y. Zou, S. Noreen, L. M. Zhao, Z. Liu, H. Ouyang, P. C. Tan, M. Yu, Y. B. Fan, Z. L. Wang, and Z. Li. Adv. Sci. **6**, 1801625 (2019).
7. W. Jiang, H. Li, Z. Liu, Z. Li, J. J. Tian, B. J. Shi, Y. Zou, H. Ouyang, C. C. Zhao, L. M. Zhao, R. Sun, H. R. Zheng, Y. B. Fan, Z. L. Wang, and Z. Li. Adv. Mater. **30**, 1801895 (2018).
8. Z. Li, H. Q. Feng, Q. Zheng, H. Li, C. C. Zhao, H. Ouyang, S. Noreen, M. Yu, F. Su, R. P. Liu, L. L. Li, Z. L. Wang, and Z. Li. Nano Energy **54**, 390 (2018).
9. C. M. Boutry, A. Nguyen, Q. O. Lawal, A. Chortos, S. Rondeau-Gagnéand, and Z. Bao. Adv. Mater. **27**, 6954 (2015).
10. Y. H. Jung, T. -H. Chang, H. L. Zhang, C. H. Yao, Q. F. Zheng, V. W. Yang, H. Y. Mi, M. Kim, S. J. Cho, D. -W. Park, H. Jiang, J. Lee, Y. J. Qiu, W. D. Zhou, Z. Y. Cai, S. Q. Gong, and Z. Q. Ma. Nat. Commun. **6**, 7170 (2015).
11. H. Li, H. -Z. Geng, Y. Meng, Y. Wang, X.-B. Xu, E. -X. Ding, J. Gao, L. -T. Chen, and S. Ma. Appl. Surf. Sci. **313**, 220 (2014).
12. C. J. Bettinger, and Z. Bao. Adv. Mater. **22**, 651 (2010).
13. M. Bortolettl, C. Rodella, R. Salvador, P. C. Miranda, and C. Miniussi, Brain Stimul. **9**, 525 (2016).
14. H. Li, X. X. Wang, W. Jiang, H. Y. Fu, X. Q. Liang, K. Zhang, Z. Li, C. C. Zhao, H. Q. Feng, J. Nie, R. P. Liu, G. Zhou, Y. B. Fan, and Z. Li. Adv. Mater. Interfaces **5**, 1701648 (2018).
15. H. Li, H. Ouyang, M. Yu, N. Wu, X. X. Wang, W. Jiang, Z. Liu, J. J. Tian, Y. M. Jin, H. Q. Feng, Y. B. Fan, and Z. Li. Small **13**, 1603642 (2017).
16. C. Wang, K. Hu, W. J. Li, H. Y. Wang, H. Li, Y. Zou, C. C. Zhao, Z. Li, M. Yu, P. C. Tan, and Z. Li. ACS Appl. Mater. Interfaces **10**, 34302 (2018).
17. L. L. Zhang, and X. S. Zhao. Chem. Soc. Rev. **38**, 2520 (2009).
18. C. F. Zhang, T. M. Higgins, S. H. Park, S. E. O'Brien, D. H. Long, J. N. Coleman, and V. Nicolosi. Nano Energy **28**, 495 (2016).
19. G. G. Jang, B. Song, L. Y. Li, J. K. Keum, Y. D. Jiang, A. Hunt, K. S. Moon, C. P. Wong, and M. Z. Hu. Nano Energy **32**, 88 (2017).
20. C. Portet, P. L. Taberna, P. Simon, and C. Laberty-Robert. Electrochim. Acta **49**, 905 (2004).